Supplemental material to this article can be found at:
http://dmd.aspetjournals.org/content/suppl/2022/05/05/dmd.122.000867.DC1
http://dmd.aspetjournals.org/content/suppl/2022/05/05/dmd.122.000867.DC2

1521-009X/51/1/54–66$35.00 dx.doi.org/10.1124/dmd.122.000867
DRUG METABOLISM AND DISPOSITION Drug Metab Dispos 51:54–66, January 2023

Stereoselective Metabolism of Bupropion to Active Metabolites in Cellular Fractions of Human Liver and Intestine[S]

Nadia O Bamfo, Jessica BL Lu, and Zeruesenay Desta

Division of Clinical Pharmacology, Indiana University School of Medicine, Indianapolis, Indiana

Received February 8, 2022; accepted April 12, 2022

ABSTRACT

Striking stereoselective disposition of the antidepressant and smoking cessation aid bupropion (BUP) and its active metabolites observed clinically influence patients' response to BUP therapy and its clinically important drug-drug interactions (DDI) with CYP2D6 substrates. However, understanding of the biochemical mechanisms responsible is incomplete. This study comprehensively examined hepatic and extrahepatic stereoselective metabolism of BUP *in vitro*. Racemic-, R-, and S-BUP were incubated separately with pooled cellular fractions of human liver [microsomes (HLMs), S9 fractions (HLS9s), and cytosols (HLCs)] and intestinal [microsomes (HIMs), S9 fractions (HIS9s), and cytosols (HICs)] and cofactors. Formations of diastereomers of 4-hydroxyBUP (OHBUP), threohydroBUP (THBUP), and erythrohydroBUP (EHBUP) were quantified using a novel chiral ultra-high performance liquid chromatography/tandem mass spectrometry method. Racemic BUP (but not R- or S-BUP) was found suitable to determine stereoselective metabolism of BUP; both enantiomers showed complete racemization. Compared with that of RR-THBUP, the *in vitro* intrinsic clearance (Cl_{int}) for the formation of SS-THBUP was 42-, 19-, and 8.3-fold higher in HLMs, HLS9 fractions, and HLCs, respectively; Cl_{int} for the formation of SS-OHBUP and RS-EHBUP was also higher (2.7- to 3.9-fold) than their R-derived counterparts. In cellular fractions of human intestine, ≥ 95% of total reduction was accounted by the formation of RR-THBUP. Ours is the first to demonstrate marked stereoselective reduction of BUP in HLCs, HIMs, HIS9 fractions, and HICs, providing the first evidence for tissue- and cellular fraction-dependent stereoselective metabolism of BUP. These data may serve as the first critical step toward understanding factors dictating BUP's stereoselective disposition, effects, and DDI risks.

SIGNIFICANCE STATEMENT

This work provides a deeper insight into bupropion (BUP) stereoselective oxidation and reduction to active metabolites in cellular fractions of human liver and intestine tissues. The results demonstrate tissue- and cellular fraction-dependent stereospecific metabolism of BUP. These data may improve prediction of BUP stereoselective disposition and understanding of BUP's effects and CYP2D6-dependent drug-drug interaction *in vivo*.

Introduction

Bupropion (BUP) is a dual inhibitor of dopamine-norepinephrine reuptake (Ascher et al., 1995), a noncompetitive nicotinic receptor antagonist (Fryer and Lukas, 1999), and an allosteric blocker of 5-hydroxytryptamine $(5\text{-HT})_{3A}$ receptors (Pandhare et al., 2017). BUP is US Food and Drug Administration approved for management of major depression, seasonal affective disorder (Jefferson et al., 2005; Foley et al., 2006), smoking cessation (Hurt et al., 1997) and, coformulated with naltrexone, for weight loss in subjects with obesity (Yanovski and Yanovski, 2015). It is also prescribed off-label for several other disorders (Dwoskin et al., 2006; Carroll et al., 2014). Patients vary in their clinical response to BUP (Thase et al., 2005) and experience adverse effects such as seizures (Davidson, 1989), dry mouth, and insomnia (Johnston et al., 2001). BUP is a strong clinical inhibitor of CYP2D6 (Kotlyar et al., 2005; Reese et al., 2008; Gheldiu et al., 2016; Todor et al., 2016).

BUP's effects and CYP2D6-mediated drug-drug interactions (DDI) vary widely among patients and the mechanisms responsible are less understood, compromising safety and efficacy. One hypothesis is that altered patterns of metabolism of BUP might contribute to this variability because BUP's effects and DDI are in most part due to active metabolites. Evidence linking BUP metabolism with its effects was first reported when BUP exhibited dose-dependent prevention of tetrabenazine-induced sedation in mice but not in rats (Soroko et al., 1977; Ascher et al., 1995). Since mice efficiently convert BUP to 4-hydroxyBUP (OHBUP) and achieved much higher plasma exposure of this metabolite than the rat, which eliminated BUP mainly through side-chain oxidation (Welch et al., 1987), it was suggested that BUP's effect was due to OHBUP.

BUP is extensively metabolized in humans. After oral administration of BUP, ~88% of the dose is excreted in urine, with <1% represented by the parent drug (Welch et al., 1987). The first human metabolite of BUP was isolated in 1979 (Schroeder, 1983). Numerous metabolites

This work was supported by National Institutes of Health/National Institute of General Medical Sciences (NIH/NIGMS) [Grants R01-R01GM121707, R35-GM145383] (Z.D.)] and N.O.B. was supported by a fellowship grant from NIH/NIGMS [Grant T32-GM008425] (Z.D.).

No author has an actual or perceived conflict of interest with the contents of this article.

dx.doi.org/10.1124/dmd.122.000867.

[S] This article has supplemental material available at dmd.aspetjournals.org.

ABBREVIATIONS: AKR, aldoketoreductase; BUP, bupropion; Cl_{int}, intrinsic clearance; DDI, drug-drug interaction; EHBUP, erythrohydrobupropion; HIC; human intestinal cytosol; HIM, human intestinal microsome; HIS9, human intestinal S9 fraction; HLC, human liver cytosol; HLM, human liver microsome; HLS9, human liver S9 fraction; 11β-HSD1, 11 beta hydroxysteroid dehydrogenase 1; MRM, multiple reaction monitoring; MS^3, multiple stage mass spectrometry; OHBUP, 4-hydroxybupropion (aka phenylmorpholinol); THBUP, threohydrobupropion; UHPLC-MS/MS, ultra-high performance liquid chromatography/tandem mass spectrometry.

have been identified to this day due to improved analytical techniques (Petsalo et al., 2007; Dash et al., 2018; Costa et al., 2019). Of these, BUP 4-hydroxylation by CYP2B6 forming an intermediate metabolite (Faucette et al., 2000; Hesse et al., 2000) that spontaneously cyclizes to a phenylmorpholinol (aka OHBUP) (Schroeder, 1983; Welch et al., 1987) and reduction at the amino ketone by 11β-hydroxysteroid dehydrogenase 1 (11β-HSD1) and other carbonyl reductases forming two amino alcohol stereoisomers, threohydroBUP (THBUP) and erythrohydroBUP (EHBUP) (Molnari and Myers, 2012; Meyer et al., 2013; Skarydova et al., 2014; Connarn et al., 2015) (Fig. 1) are of greatest interest. These metabolites are pharmacologically active based on preclinical [reviewed in Costa et al., (2019)] and clinical studies (Zhu et al., 2012; Laib et al., 2014) and mediate clinical BUP-CYP2D6 interaction (Sager et al., 2017).

In addition, the steady state plasma exposures of OHBUP, THBUP, and EHBUP after BUP therapy greatly exceed that of BUP (up to 22-, 12-, and 2.7-fold higher, respectively) (Daviss et al., 2005; Benowitz et al., 2013), with unexplained wide variability among patients that appears to predict treatment outcomes (Zhu et al., 2012; Laib et al., 2014). BUP is a chiral drug clinically administered as a racemic mixture of equimolar amounts of R- and S-BUP and biotransformation to these active metabolites introduces additional chiral centers, generating six diastereomers. Although there are no clinical studies showing direct associations of circulating stereoisomers of BUP and its metabolites with response, tolerability, or DDIs, there is compelling evidence from preclinical studies that the pharmacological activity (Reese et al., 2008; Carroll et al., 2014; Masters et al., 2016a; Sager et al., 2016; Dash et al., 2018; Costa et al., 2019) and DDI risk (Reese et al., 2008; Sager et al., 2016; Tanaudommongkon et al., 2019) of BUP and its metabolites are stereospecific. For example, the IC_{50} value for the inhibition of dopamine and norepinephrine uptake by SS-OHBUP was ~12- and ~19-fold lower, respectively, than that of RR-OHBUP (Damaj et al., 2004). SS-OHBUP also shows a greater potency (as potent as racemic BUP) than RR-OHBUP *in vivo* in a mouse model of depression and in antagonism of acute nicotine effects in mice (Damaj et al., 2004).

Although less studied compared with diastereomers of OHBUP, there is evidence that threo- and erythro-hydroBUP also contribute to pharmacological activity and BUP toxicity (Silverstone et al., 2008). Similarly, *in vitro* data suggest that inhibition of CYP2D6 is in part mediated by BUP metabolites (Reese et al., 2008), and this DDI effect of BUP and its metabolites is stereoselective (e.g., the half-maximum inhibitory concentration, IC_{50}; and the sissociation constant of the enzyme-inhibitor complex, K_i values for the inhibition of CYP2D6 by S-BUP was ~14-fold and ~7-fold lower , respectively, than that of R-BUP; and EHBUP is ~3- to 5-fold more potent than THBUP) (Reese et al., 2008; Sager et al., 2017; Tanaudommongkon et al., 2019).

Marked stereoselective disposition of BUP and its active metabolites has been observed clinically (Masters et al., 2016a; Kharasch et al., 2020). Yet, understanding of *in vitro* stereoselective metabolism of BUP remains incomplete. The limited studies reported on BUP stereoselective oxidation and/or reduction (Coles and Kharasch, 2008; Wang et al., 2020) did not rigorously address the impact of racemization of BUP on estimation of kinetic parameters, and the scope of these studies was limited to enzymes localized in the liver. BUP reduction to THBUP and/or EHBUP occurs in human liver cytosols and in cellular fractions of human intestine (Skarydova et al., 2014; Connarn et al., 2015). Whether reduction of BUP in these cellular fractions is stereospecific remains unexplored.

In this study, we hypothesized that stereoselective metabolism of BUP in cellular fractions of hepatic and extrahepatic (intestine) tissues explains the marked stereoselective disposition of BUP and its active metabolites observed *in vivo*. The main objectives of this study were to develop a reliable chiral ultra-high performance liquid chromatography/tandem mass spectrometry (UHPLC/MS/MS) method to quantify stereoisomers of BUP and metabolites, rigorously assess the extent of racemization and identify proper conditions for *in vitro* stereoselective study, and characterize stereoselective metabolism of BUP in human subcellular fractions of liver and intestine.

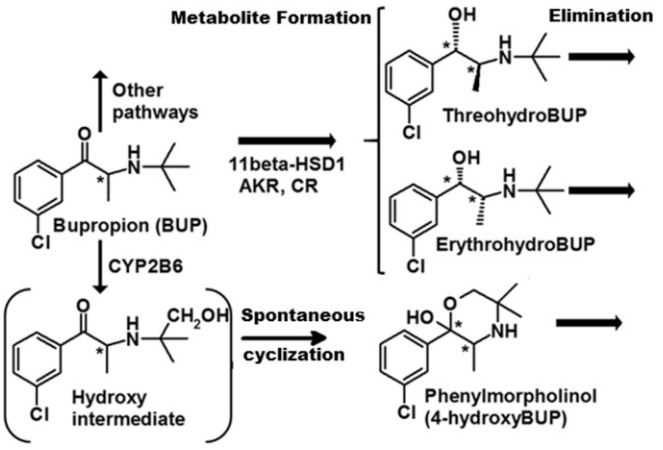

Fig. 1. Human metabolism of bupropion (BUP) to active metabolites. BUP is extensively metabolized generating several metabolites. Of the numerous metabolites identified so far, CYP2B6 mediated 4-hydroxylation of the tert-butyl group forming an intermediate hydroxyl metabolites that spontaneously cyclizes to a phenylmorpholinol (aka 4-hydroxyBUP) and reduction of the amino ketone group by 11β-hydroxysteroid dehydrogenase 1 (11β -HSD1), aldoketo-reductases (AKRs), and other carbonyl reductases (Connarn et al., 2015) forming two amino alcohol stereoisomers, namely threo- and erythro-hydroBUP, are of greatest interest in understanding BUP's clinical effect, toxicity, and CYP2D6-dependent drug interaction. BUP is clinically used as a racemic mixture of R- and S-BUP (50%:50%) and biotransformation creates additional chiral centers, generating multiple stereoisomers, each with distinct pharmacological profile. *Chiral centers

Materials and Methods

Chemicals. Racemic-, R-, and S-bupropion (BUP); RR-hydroxybupropion (RR-OHBUP); SS-hydroxybupropion (SS-OHBUP); racemic erythrohydroBUP (EHBUP); RR-threohydrobupropion (RR-THBUP); and SS-threohydrobupropion (SS-THBUP) were obtained from Toronto Research Chemicals Inc. (North York, ON, Canada). Nevirapine was a generous gift from National Institutes of Health HIV Reagent Program. NADPH was purchased from Dot scientific inc. (Burton, MI). All the other solvents and chemicals were purchased from Fishers Scientific (Hampton, NH) and were of high-performance liquid chromatography/mass spectrometry (LC/MS/MS) grade.

Cellular Fractions of Human Liver and Intestine. Pooled human liver microsomes from 50 donors with mixed sex [average age: 47 years old (range: 5–83)] (20 mg/ml), pooled human liver S9 (HLS9s) from 50 donors with mixed sex [average age: 53 (range 26–78)] (20 mg/ml), and human liver cytosol (HLCs) from 50 donors with mixed sex [age range 5–73) (10 mg/ml) were purchased from Xenotech LLC (Kansas City, KS). Pooled human intestinal microsomes (HIMs) from 15 donors with mixed sex [average age: 54 years old (range: 26–69)] (10 mg/ml), human intestine S9 (HIS9) from 15 donors with mixed sex [average age: 54 (range 26–69)] (4 mg/ml), and human intestine cytosol (HIC) from 13 donors with mixed sex [average age: 40 years old (range 18–55)] (4 mg/ml) were purchased from Xenotech. All cellular fractions of human liver and intestine were stored at -80°C until used.

UHPLC/MS/MS Method. Previously, we have developed the first chiral HPLC/MS/MS method that allowed chromatographic separation and simultaneous quantification of BUP and its active metabolites (Masters et al., 2016b).

Building on this initial work, a further improved chiral UPLC/MS/MS method was developed to separate and quantify stereoisomers of BUP, OHBUP, EHBUP, and THBUP. Compared with the previous method (Masters et al., 2016b), the new method had several advantages, including better chromatographic resolution of the stereoisomers, short retention times, no need for extraction of samples,

small sample and injection volumes, and suitability for high throughput with 96-well plate format. The MS/MS analysis was performed on QTRAP 6500+ mass spectrometer [Applied Biosystem/MDS Sciex (Masters et al., 2016b), Foster City, CA] equipped with a turbo V ion spray source and coupled with a UHPLC system consisting of two Sciex ExionLC AD pumps, an AD autosampler and AD column oven, AD degasser, and a UPLC controller. Data were acquired using Analyst software (version 1.6.3; AB Sciex) and quantification was made via MultiQuant software (version 3.0.2; AB Sciex).

For MS/MS optimization experiments, stock solutions of nevirapine (internal standard), racemic BUP, S-BUP, R-BUP, RR-OHBUP, SS-OHBUP, RR-THBUP, and SS-THBUP were dissolved in methanol (10 μg/ml each). Since RS-EHBUP and SR-EHBUP were not available to us, we used racemic EHBUP. Serial dilutions of each analyte were performed from the stock solutions in methanol and mobile phase. MS optimization was achieved via adjustment of both the compound- and instrument-dependent parameters for the analytes for multiple reaction monitoring (MRM) and multiple stage mass spectrometry (MS^3) when needed in positive mode. The analytes were optimized at a source temperature of 550°C for MRM and 600°C for MS^3, under unit resolution for quadrupole 1 and 3 and unit for MS3, and were given a delay of 0.1s. Optimal gas pressures for all analytes including the internal standard were collision gas, medium; curtain gas, 25 psi; ion source gas (1), 35 psi; ion source gas (2), 20 psi; ion spray voltage, 5500V; and pause between mass ranges, 5.007 millisecond. MS^3 conditions were dynamic fill time, Q3 entry barrier of 8V, and MS/MS/MS fragmentation excitation time of 25 milliseconds. Further MS/MS and MS^3 specifications are listed in Supplemental Table 1.

Chromatographic separation of stereoisomers of BUP, OHBUP, EHBUP, and THBUP was achieved using a Phenomenex (Masters et al., 2016b) AMP LC column (150 × 4.6 mm; 3.0μm) and a mobile phase consisting of mobile phase A (5 mM ammonium bicarbonate, pH 11) and mobile phase B (methanol) delivered at a gradient flow rate of 0.8 ml/min. The gradient elution of mobile phase A: mobile phase B was: 40%:60% (0–3 minutes); within 0.01 minute increased to 25%:75% and via linear gradient to 5%:95% (3.01–12 minutes); and then back to initial condition (40%:60%) to equilibrate the column (12.01–13 minutes). The injection volume was 10μl. Before and after each injection, the needle was washed with 25% acetonitrile, 25% 2-propanol, and 50% water with 0.1% formic acid. BUP and its metabolites were quantified using MRM and MS^3 in positive mode (Supplemental Table 1). MS^3 was only used for diastereomers of THBUP and EHBUP to avoid crosstalk. The molecular mass and MS/MS fragmentation patterns (parent and daughter ions) of each stereoisomer (R- and S-BUP, SS- and RR-OHBUP, SS- and RR-THBUP, and RS- and SR-EHBUP) were the same (Supplemental Table 1). Therefore, quantification of each stereoisomer pair was performed after chiral chromatographic separation. A typical MRM trace chromatogram of stereoisomers of BUP and its primary metabolites after direct injection of authentic standards into a chiral UHPLC-MS/MS system shows that each stereoisomer was effectively separated and eluted within 10 minutes retention time (Supplemental Fig. 1).

The incubation-generated metabolites were quantified using commercially available authentic metabolite standards with a dynamic assay range of 0–2000 nM. The instrument response was linear with respect to increasing analyte concentration over the standard curve range used. The lower limit of quantification was 1 nM for RR and SS OHBUP and 0.1 nM for SR and RS-EHBUP, as well as RR and SS-THBUP. Inter-day and intra-day assay accuracy was evaluated using MultiQuant software. Standard and quality control samples were deemed acceptable if within 20% and 10% of the nominal value, respectively, whereas the precision was greater than >90% (% CV<10).

General Incubation Conditions. Incubation and sample processing was performed in a 96-well plate (Thomas Scientific, Swedesboro, NJ). Stock solutions (1 mg/ml) of each substrate (racemic-, R-, or S-BUP) dissolved in methanol were added to a 0.65 ml disposable culture tube. Methanol was removed by evaporation in speed vacuum (Thermo Fisher Scientific, Asheville, NC) and reconstituted with 400 μl of 200 mM phosphate buffer (Irvine et al., 1999) and then serially diluted in phosphate buffer to the required concentration. Into each well, 100 μl containing the substrate and 30 μl of cellular fraction of human liver and intestine (HLMs, HLS9s, HLCs, HIMs, HIS9s, or HICs), all diluted in phosphate buffer on ice, was added. The mixture was prewarmed on Isotemp heater (Fisher Scientific, Waltham, MA) for 5 minutes at 37°C. Reaction was initiated by adding a 20 μl of NADPH (final concentration, 1 mM) in phosphate buffer (total incubation volume 150 μl) and allowed to proceed for the specific incubation time at 37°C. The reaction was terminated by transferring 100 μl of incubation solution into another clean 96-well plate (1.1 ml tubes) containing 20 ng/ml nevirapine (internal standard) in 300 μl of ice cold methanol solution. The mixture was shaken for 2 minutes at 2500 rpm on a bench mixer (Benchmark, Tempe, AZ) and centrifuged for 20 minutes at 4°C on AllgeraTM 6R centrifuge (Beckmen coulter, Brea, CA). Then, 190 μl of supernatant was transferred into a new 96-well plate (0.65 ml tube) from which 10 μl of supernatant was injected into the UHPLC/MS/MS system described above. Before proceeding with subsequent experiments, pilot incubation experiments were performed to define optimal conditions for incubation and UHPLC/MS/MS analysis. Racemic-, R-, or S-BUP (10 μM) was incubated with HLMs (0.4 mg/ml) for 20 minutes and 1 mM NADPH at 37°C. Negative control incubations consisting of no substrate, no cofactors, or no microsomes (bovine serum albumin was used instead) were run in parallel and processed as above.

To ensure linearity of metabolite formation and prevent greater than 20% substrate depletion, racemic-, R-, or S-BUP (10 μM) was incubated separately with a range of final protein concentrations (0.2, 0.4, 0.8, and 1 mg/ml) of cellular fractions of human liver (HLMs, HLS9s, and HLCs) and intestine (HIM, HIS9, and HICs) and NADPH for 0, 5, 10, 20, 30, and 60 minutes at 37°C. Twenty minutes of incubation (all cellular fractions), and 0.4 mg protein/ml (HLM, HIM, and HLS9) and 0.2 mg protein/ml (HIS9, HIC, and HLC) were selected and represented linear conditions to minimize sequential metabolism while ensuring assay sensitivity.

Kinetic Analysis. Kinetics for the stereoselective metabolism of BUP were assessed in HLMs using racemic BUP and its enantiomers, S- and R-BUP, as substrates. A range of concentrations of racemic BUP (1.96–4000 μM), R-BUP (0.98–2000 μM), and S-BUP (0.98–2000 μM) were incubated in duplicate with HLMs and 1 mM NADPH for 20 minutes at 37°C. Reaction was terminated and processed as above. Metabolites formed from racemic BUP and its enantiomers (diastereomers of 4-OHBUP, THBUP, and EHBUP) were measured using a chiral assay (see *UHPLC/MS/MS Method* section). Formations of diastereomers of OHBUP (SS- and RR-OHBUP), THBUP (SS- and RR-THBUP), and EHBUP (RS- and SR-EHBUP) were chromatographically separated and quantified using the chiral UHPLC/MS/MS method describe above. This approach was instrumental in assessing the extent of racemization of R- and S-BUP as compared with racemic incubations and enabled to define the most appropriate conditions to study stereoselective kinetics of BUP metabolism with minimal chiral inversion. Based on the initial data obtained, it was deemed more appropriate to use the racemic mixture that contains equimolar concentrations of R- and S-BUP as a substrate to assess stereoselective metabolism of BUP, and thus was used in the subsequent kinetic experiments in all cellular fractions (HLMs, HLS9 fractions, HLCs, HIM, HIS9 fractions, and HICs). In addition, since the initial data seemed to show less racemization in terms of R-BUP derived metabolite formation when S-BUP was used as a substrate and kinetics for S-BUP metabolism were included as a positive control. Thus, racemic BUP and S-BUP (range of concentrations described above) was incubated with HLMs, HLC, HLS9 or HIMs, HIS9, and HICs (see *General Incubation Conditions*, for concentrations and conditions). Reaction was terminated and processed as above. Metabolites formed (diastereomers of OHBUP, THBUP, and EHBUP) were measured using a chiral assay (see *UHPLC/MS/MS Method* section).

Data Analysis. Kinetic analyses were performed by initial visual examination of Eadie-Hofstee plots (velocity versus velocity/substrate concentrations) to help guide the appropriate equations to use. The formation rate of metabolite (V) versus substrate concentration was plotted and fit to appropriate kinetic equations (the simple single-site Michaelis-Menten, Hill, two-site binding, and substrate inhibition equations) using a nonlinear regression analysis in GraphPad Prism 7 (Version 7.01, San Diego, CA; www.graphpad.com). Based on the dispersion of residuals and standard errors of the parameter estimates, the Michaelis-Menten equation ($v = V_{max} * [S]/K_m + [S]$) best fit each data set and kinetic parameters [apparent maximum formation rate (V_{max}) and the Michaelis-Menten constant (K_m)] were estimated. *In vitro* intrinsic formation clearance of the metabolite (Cl_{int}) was calculated as the ratio of the V_{max} and K_m (V_{max}/K_m). Data are presented as mean ± S.D. or as averages of duplicate experiments.

Prediction of Stereoselective Organ Clearances. Cl_{int} in the liver was scaled using liver weight of 1800 g (Davies and Morris, 1993) and scaling factors; MPPGL = 40 mg microsomal protein/g liver, CPPGL = 81 mg cytosolic protein/g liver (Cubitt et al., 2009, 2011), and HLS9 = 121 mg protein/g liver (Nishimuta et al., 2014) for HLMs, HLCs, and HLS9 fractions, respectively.

Protein binding in incubation was assumed to be negligible and unbound fraction was assumed to be 1 (Sager et al., 2016). Small intestine weight of 809 g (Paine et al., 1997) was used to scale Cl_{int} in the intestine, along with scaling factors; MPPI = 20.6 mg microsomal protein/g intestine, CPPGI = 18 mg cytosolic protein/g intestine (Cubitt et al., 2009, 2011), and HIS9 = 38.6 mg protein/g intestine (Nishimuta et al., 2014) for HIMs, HICs, and HIS9 fractions, respectively. The hepatic (H) blood clearance of R- and S-BUP ($CL_{h,R}$; and $CL_{h,S}$) was estimated using the well stirred model in eqs. 1 and 2, respectively. The intestinal clearance of R- and S-BUP ($CL_{intestine,R}$ and $CL_{intestine,S}$) was estimated using the well stirred model in eqs. 3 and 4, respectively. Blood flow values (Q) of 1450 ml/min to the liver and 1100 ml/min to the gut (Davies and Morris, 1993) were used. Fraction unbound in blood (fu_B) was derived by multiplying the fraction unbound in plasma (FuP) by blood:plasma ratio (BP). Fup and BP values for R and S-BUP were obtained from literature (Sager et al., 2016).

$$CL_{h,R} = \frac{Q * fuB * CLint,R,H}{Q + (fuB * CLint,R,H)} \quad (1)$$

$$CL_{h,S} = \frac{Q * fuB * CLint,S,H}{Q + (fuB * CLint,S,H)} \quad (2)$$

$$CL_{intestine,R} = \frac{Q * fuB * CLint*,R,intestine}{Q + (fuB * CLint,R,intestine)} \quad (3)$$

$$CL_{intestine,S} = \frac{Q * fuB * CLint,S,intestine}{Q + (fuB * CLint,S,intestine)}. \quad (4)$$

Results

Chiral UHPLC/MS/MS Assay of BUP and Its Metabolites

As described in the *Methods* section, a much improved chiral UHPLC/MS/MS method over the previously reported method (Masters et al., 2016b) was developed allowing chromatographic separation and simultaneous quantification of all stereoisomers of BUP and its active metabolites. A representative MRM and MS^3 trace chromatogram of BUP and its metabolites after incubation of racemic BUP (31.2 μM) with HLMs and NADPH for 20 minutes at 37°C is shown in Fig. 2. As with direct injection of authentic standards (Supplemental Fig. 1), effective chiral separation of the metabolites generated from incubations of racemic-, R-, and S-BUP was achieved within 12 minutes. BUP undergo 4-hydroxylation in HLMs to form an intermediate hydroxy metabolite that spontaneously cyclizes to phenylmorpholinol (aka 4-OHBUP), creating a second chiral center. Although four diastereomers of this OHBUP are theoretically expected (SS-, RR-, RS-, and SR-OHBUP), only two transdiastereomers, *SS*- and *RR*-OHBUP, were separated and detected. None of the metabolites listed in Fig. 2 were detected in the negative control experiments (Data not shown).

Assessment of Racemization (Chiral Inversion)

Effective chromatographic separation and simultaneous quantification of all stereoisomers of BUP and its active metabolites was achieved after direct injection of authentic standards (Supplemental Fig. 1) and in microsomal incubations of racemic-, S-, and R-BUP (Fig. 2). The results depicted in Fig. 3 and Table 1 show complete racemization of R-BUP as shown by appreciable formation of S-derive metabolites (SS-OHBUP, RS-EHBUP, and SS-THBUP) when R-BUP was incubated with pooled HLMs separately. Broadly similar Cl_{int} of RS- versus SR-EHBUP, and SS-OHBUP versus RR-OHBUP, was observed. Interestingly, the Cl_{int} for the formation of S-BUP derived SS-THBUP was even substantially higher (~42-fold) compared with that of R-BUP derived RR-THBUP in R-BUP incubations. On the other hand, the ratios for metabolic clearance of S-BUP derived metabolites (RS-EHBUP, SS-THBUP, and SS-OHBUP) to the corresponding R-BUP derived

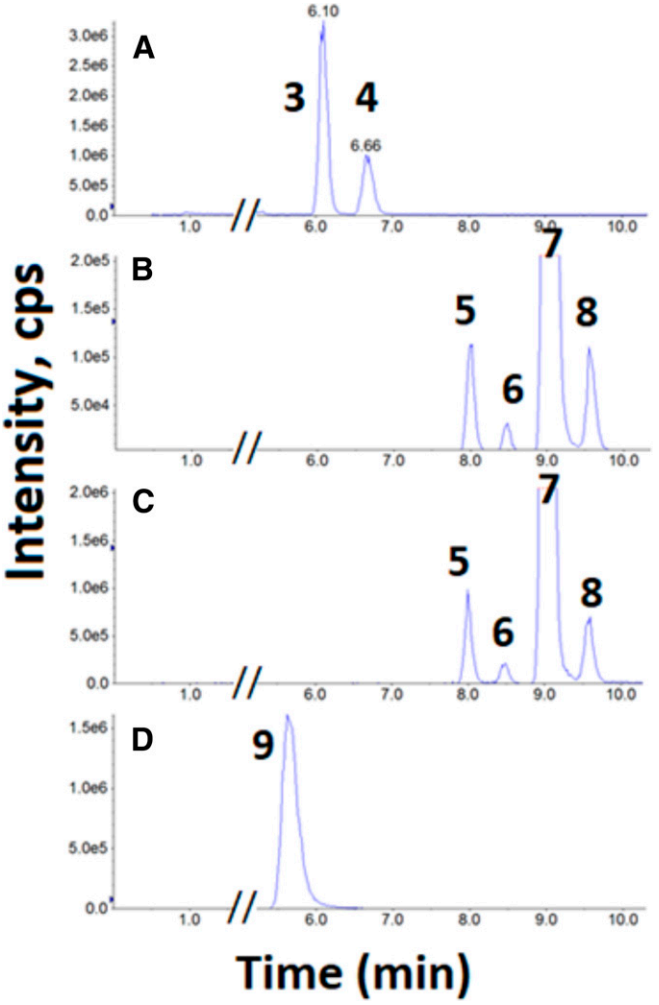

Fig. 2. MRM (A–B) and MS^3 (C) trace chromatograms of BUP metabolites after incubations of racemic BUP (31.2 μM) with HLMs and NADPH for 20 minutes at 37°C. (A) MRM of SS-OHBUP (3) and RR-OHBUP (4); (B) MRM of RS-EHBUP (5), SR-EHBUP (6), SS-THBUP (7), and RR-THBUP (8); and (C) MS^3 of RS-EHBUP (5), SR-EHBUP (6), SS-THBUP (7), and RR-THBUP (8). (D) shows MRM of the internal standard, nevirapine (9). The MS^3 analysis (C) for diastereomers of threohydroBUP (THBUP) and erythrohydroBUP (EHBUP) was needed to avoid crosstalk.

metabolite (SR-EHBUP, RR-THBUP, and RR-OHBUP) was 8.9-, 141.4-, and 7.3-fold higher, respectively, in incubations of S-BUP with pooled HLMs (Fig. 3 and Table 1). As judged by the rate of formation of S- and R-BUP derived metabolites in S-BUP incubations with pooled HLMs, racemization of S-BUP metabolism was initially suggested to be minimal (Table 1). The *in vitro* Cl_{int} for the formation of S-BUP derived metabolites (RS-EHBUP, SS-THBUP, and SS-OHBUP) after incubations of racemic BUP containing equimolar concentrations of R- and S-BUP with pooled HLMs broadly concurred with the values obtained when S-BUP was incubated separately. The *in vitro* Cl_{int} for the formation of R-BUP derived metabolites (SR-EHBUP, RR-THBUP, and RR-OHBUP) was slightly higher (2.3-, 1.7-, and 2.9, respectively) than the values generated from incubations of R-BUP separately (Fig. 3 and Table 1). This chiral assay along with rigorous assessment of racemization allowed us to properly determine the effect of racemization on estimation of enzyme kinetic parameters and define/select the optimal experimental approaches and assay conditions to study stereoselective metabolism of BUP *in vitro*. Thus, based on the S- and R-BUP derived metabolites formed, racemic

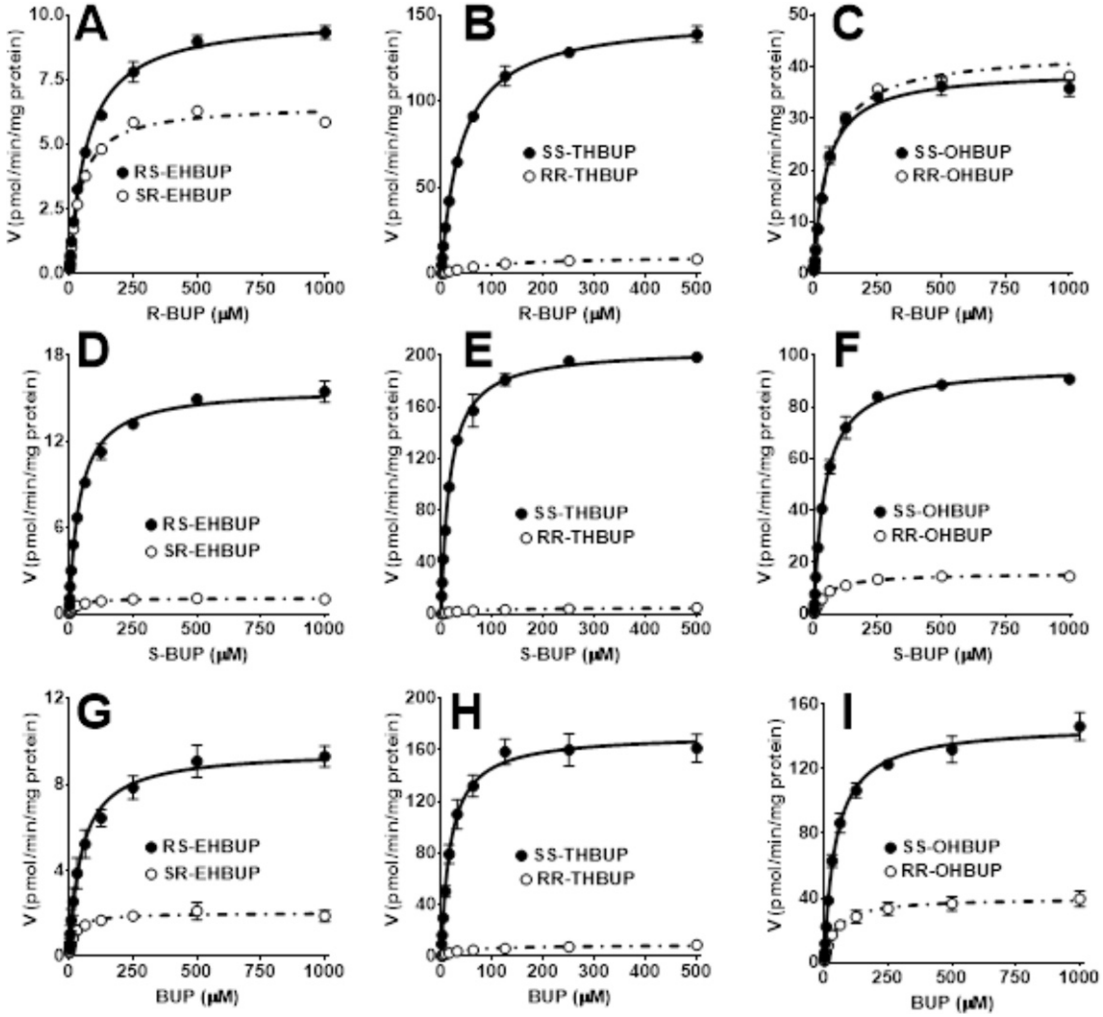

Fig. 3. Comparison of rates of metabolism of racemic-, S-, and R-BUP and assessment of racemization in incubations of HLMs. The kinetics for the metabolism of S-BUP (0.98–2000 μM), R-BUP (0.98–2000 μM), and racemic BUP (1.96–4000 μM) were determined by incubating each substrate separately with HLMs (0.4 mg protein/ml) and 1 mM NADPH for 20 minutes at 37°C. Metabolites formed (SR-EHBUP, RS-EHBUP, RR-THBUP, SS-THBUP, RR-OHBUP, and SS-OHBUP) from each substrate (racemic-, S-, and R-BUP) were monitored using chiral assay (see *Methods* section). (A–C) R-BUP incubation; (D–F) S-BUP incubation; and (G–I) racemic BUP incubation. Corresponding kinetic parameters derived from fitting the formation rate of metabolite (V) versus substrate concentration to the Michaelis-Menten equation using a nonlinear regression analysis in GraphPad Prism 7 (Version 7.01, San Diego, CA; www.graphpad.com) are listed in Table 1.

BUP was selected as an appropriate substrate to study stereoselective metabolism *in vitro*. S-BUP was used as an internal positive control in all kinetic experiments.

During the kinetic experiments, we noted that RR-THBUP was the major metabolite formed in incubations of racemic and S-BUP with cellular fractions of human intestine (see below). This observation raised the question whether the differences in extent of racemization of R- and S-BUP in terms of metabolite formation was due to differences in chiral inversion of R-BUP to S-BUP or vice versa. Thus, each enantiomer was separately incubated with pooled HLMs and cofactors followed by measuring both R- and S-BUP in each incubation after chiral separation. The MRM trace chromatograms presented in Fig. 4A show that R-BUP is quickly converted to S-BUP in R-BUP incubations, and similarly S-BUP was efficiently converted to R-BUP in S-BUP incubations. The ratio of R- to S-BUP and S- to R-BUP in R- and S-BUP incubations, respectively, was close to unity across a range of substrate concentrations (Fig. 4B). The observed difference in racemization in terms of metabolite formation between R- and S-BUP was therefore not due to differences in extent of racemization of R-BUP to S-BUP or S-BUP to R-BUP. The total Cl_{int} for the formation of S- and R-BUP derived metabolites in HLMs accounted for 90.7% and 9.3% of the total racemic BUPmetabolism (see below). Given the effective racemization of S-BUP to R-BUP and vice versa, the difference in the formation of S- and R-BUP derived metabolites in incubations of S- and R-BUP is simply a reflection of differences in rate of metabolism in HLMs.

For these reasons, the kinetics for the stereoselective metabolism of racemic BUP are presented in the following sections of the manuscript for the sake of consistency and clarity, whereas the kinetics data generated from the metabolism of S-BUP were only used as a marker of tissue selective differences in rates of metabolism.

Stereoselective Metabolism of BUP in HLMs, HLS9 Fractions, and HLCs

Stereospecific metabolism of BUP was characterized in cellular fractions derived from human liver.

Pooled HLMs. The kinetics for stereoselective metabolism of racemic BUP were determined in pooled HLMs (Fig. 5 and Table 2, upper panel). The average K_m values for the formation of RR- and SS-OHBUP

TABLE 1

Comparison of kinetic parameters for the formation of metabolites from racemic-, S-, and R-BUP in HLMs.

A range of concentrations of racemic BUP (1.96–4000 μM), S-BUP (0.98–2000 μM), and R-BUP (0.98–2000 μM) with HLMs (0.4 mg/ml) and 1 mM NADPH for 20 min at 37°C. Metabolites formed (RS-EHBUP and SR-EHBUP; RR-THBUP and SS-THBUP; and RR-OHBUP, SS-OHBUP) from incubation of each substrate were monitored using chiral assay (see Methods section). Formation rates of metabolites from: R-BUP incubations (upper panel); S-BUP incubations (middle panel); and racemic-BUP incubations (lower panel).

Substrate	Metabolites	V_{max} (pmol/min/mg protein)	K_m (μM)	Cl_{int} (μl/min/mg protein)	[a]Cl_{int} Ratios
R-BUP	RS-EHBUP	9.97	67.9	0.147	0.97
	SR-EHBUP	6.54	43.2	0.151	
	SS-THBUP	149.1	39.0	4.194	41.9
	RR-THBUP	10.21	102.8	0.10	
	SS-OHBUP	39.33	48.4	0.81	1.1
	RR-OHBUP	42.91	58.4	0.77	
S-BUP	RS-EHBUP	15.73	40.79	0.39	8.7
	SR-EHBUP	1.109	25.3	0.044	
	SS-THBUP	199.4	15.3	13.01	141.4
	RR-THBUP	5.698	61.9	0.092	
	SS-OHBUP	96.16	42.6	2.26	7.3
	RR-OHBUP	15.88	51.6	0.31	
Racemic BUP	RS-EHBUP	9.59	48.1	0.2	2
	SR-EHBUP	2.03	20.4	0.1	
	SS-THBUP	166.2	16.5	10.17	63.6
	RR-THBUP	11.1	71.2	0.16	
	SS-OHBUP	147.3	44.6	3.30	3.7
	RR-OHBUP	40.07	45.1	0.89	

[a]C_{int} ratios for each diastereomer pair: RS-EHBUP/SR-EHBUP, SS-THBUP/RR-THBUP, and SS-OHBUP/RR-OHBUP.

were comparable (42.5 versus 42.3 μM, respectively). The V_{max} and the *in vitro* intrinsic clearance [Cl_{int} (V_{max}/K_m)] for the formation of SS-OHBUP was ~3.4-fold higher than the formation of RR-OHBUP. Marked stereoselective reduction of BUP to THBUP and EHBUP was observed; the K_m, V_{max}, and Cl_{int} values for the formation of SS-THBUP were 2.3-fold lower and 18.6- and 42.1-fold higher, respectively, compared with the formation of RR-THBUP. The V_{max} and Cl_{int} values for the formation of RS-EHBUP, respectively, were approximately 5- and 3-fold higher than the formation of SR-EHBUP. The total *in vitro* Cl_{int} for the metabolism of BUP via both oxidation and reduction in pooled HLMs was 14.36 μl/min/mg protein. Since the total Cl_{int} via reduction to both THBUP and EHBUP was 9.85 μl/min/mg protein and total Cl_{int} for the formation of OHBUP was 4.51 μl/min/mg protein, reduction (to THBUP, 65.8% and EHBUP, 2.8%) accounts for 68.6% and 4-hydroxylation for 31.4% of the total metabolic clearance. Relative to the total metabolic clearance (oxidation + reduction), the Cl_{int} for the formation of SS-THBUP, SS-OHBUP, RR-OHBUP, RS-EHBUP, RR-THBUP, and SR-EHBUP was 64.3%, 24.3%, 7.1%, 2.1%, 1.5%, and 0.7% of total metabolic clearance. The total Cl_{int} for the formation of S-BUP derived metabolites was 13.03 μl/min/mg protein of which the Cl_{int} for the formation of SS-THBUP accounted for 70.9% followed by SS-OHBUP (26.8%) and RS-EHBUP (2.3%). The total Cl_{int} for the formation of R-BUP derived metabolites was 1.34 μl/min/mg protein of which 76% was accounted by Cl_{int} for the formation of RR-OHBUP, 16.4% by RR-THBUP, and 7.6% by SR-EHBUP. The total in vitro Cl_{int} and predicted *in vivo* hepatic Cl_{int} of S-BUP derived metabolites (both oxidation and reduction) was 9.8-fold higher than the total metabolic clearance of R-BUP metabolism. Thus, 90.7% and ~9.3% of the total formation clearance of racemic BUP (oxidation + reduction) was due to S- and R-BUP metabolism, respectively.

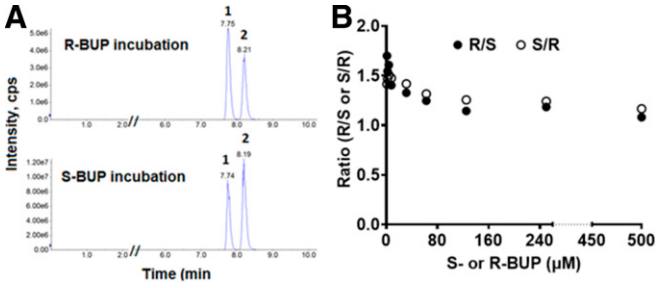

Fig. 4. Extent of racemization of R-BUP to S-BUP and vice versa in incubations of R- or S-BUP in HLMs. A range of concentrations of R- (0.98–2000 μM) and S-BUP (0.98–2000 μM) were incubated with HLMs (0.4 mg protein/ml) and 1 mM NADPH for 20 minutes at 37°C. Both S- and R-BUP were quantified in each incubation after chiral separation. (A) MRM trace chromatograms of R- and S-BUP in incubation of 15.6 μM R-BUP (upper panel) and 15.6 μM S-BUP (lower panel); and (B) ratio of R-BUP/S-BUP in R-BUP incubations and S-BUP/R-BUP in S-BUP incubation across a range of concentrations used to study saturation kinetics.

Pooled HLS9 Fractions. Stereoselective reduction of BUP to THBUP and EHBUP as well as 4-hydroxylation to OHBUP was determined in HLS9 fractions and compared with those data obtained from HLMs. Representative plots of stereospecific metabolism of racemic BUP in HLS9 fractions are depicted in Fig. 5 (middle panel), and the kinetic parameters are summarized in Table 2 (middle panel). Although the total *in vitro* Cl_{int} for the metabolism of BUP via both oxidation and reduction in pooled HLS9 fractions (14.03 μl/min/mg protein) was comparable with that observed in HLMs (14.36 μl/min/mg protein), quantitative difference in the contribution of reduction and 4-hydroxylation of BUP to the total Cl_{int} was noted. Reduction to both THBUP and EHBUP (13.53 μl/min/mg protein) and 4-hydroxylation to OHBUP (0.498 μl/min/mg protein) accounted for 96.4% and 3.6% of the total Cl_{int} (oxidation + reduction) in HLS9 fractions (in HLMs, this was 68.6% and 31.4% of the total metabolic clearance, respectively). This difference was largely due to substantially lower rate of 4-hydroxylation (10.6- and 8.4-fold lower V_{max} for the formation of SS- and RR-OHBUP, respectively) in HLS9 fractions compared with the V_{max} values in HLMs, and accordingly, the Cl_{int} values in HLS9 fractions were 9.6- and 7.6-fold lower, respectively, than those in HLMs; K_m values among the two enzyme sources were similar (~38 μM for both SS- and RR-OHBUP in HLS9 fractions and ~42 μM in HLMs) (Table 2, upper and middle panel). Despite this, the extent of stereoselectivity in 4-hydroxylation (~2.7-fold higher for the formation of SS-OHBUP than the formation for RR-OHBUP) in HLS9 fractions was comparable to that in

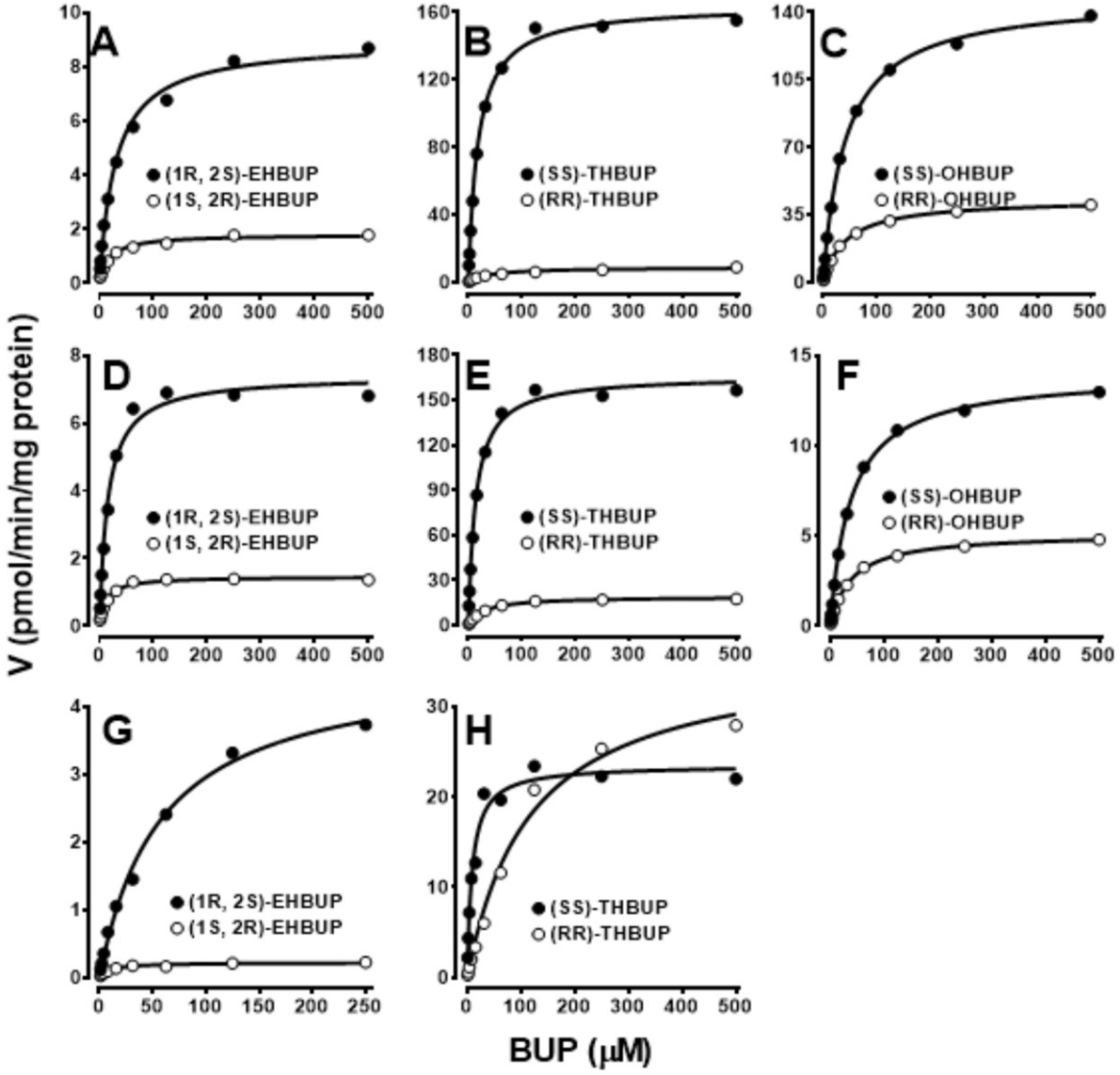

Fig. 5. Stereoselective metabolism of BUP in human liver microsomes, HLS9 fractions, and HICs. Increasing concentrations of racemic BUP (1.96–4000 μM) consisting of 50%/50% of R- and S-BUP was incubated in duplicate with cellular fractions of human liver (0.4 mg protein/ml pooled HLMs or pooled HLS9 fractions: or 0.2 mg protein/ml HLCs) for 20 minutes at 37°C. Formation rates of diastereomers of OHBUP, THBUP, and EHBUP versus BUP concentrations (0.98–500 μM corresponding to R- and S-BUP) were best fit to a Michaelis Menten equation. Formation rates of BUP metabolites in HLMs (upper panel, A–C), HLS9 fractions (middle panel, D–F), and HLCs (lower panel, G–H) are shown. Each point represents an average of duplicate incubations. Corresponding kinetic parameters derived from fitting the formation rate of metabolite (V) versus substrate concentration to the Michaelis-Menten equation using a nonlinear regression analysis in GraphPad Prism 7 (Version 7.01, San Diego, CA; www.graphpad.com) are listed in Table 2.

HLMs (~3.4-fold). As in HLMs, the greatest stereoselectivity was observed with the formation of diastereomers of THBUP. The K_m, V_{max}, and Cl_{int} values for the formation of SS-THBUP were 2.2-fold lower and 8.7- and 19.2-fold higher, respectively, compared with the formation of RR-THBUP (Table 2, middle panel); this difference was less pronounced than that observed in HLMs (18.6- and 42.1-fold higher V_{max} and Cl_{int} for the formation of SS-THBUP, respectively). The extent of stereoselectivity in the formation of EHBUP (5.1- and 3.9-fold higher V_{max} and Cl_{int} for the formation of RS-EHBUP, respectively, than that of SR-EHBUP) in HLS9 fractions is similar to that observed in HLMs (Table 2, middle panel). Relative to the total metabolic clearance via oxidation + reduction, the Cl_{int} for the formation of SS-THBUP was the highest (87.6% of total) followed by RR-THBUP (4.6% of total), RS-EHBUP (3.4% of total), SS-OHBUP (2.6% of total), RR-OHBUP (1% of total), and SR-EHBUP (0.9% of total). This pattern was somewhat different from those data generated using HLMs (SS-THBUP⋙>SS-OHBUP⋙ RR-OHBUP>RS-EHBUP ≈ RR-THBUP ≈ SR-EHBUP). Relative to the total metabolic clearance of S-BUP derived metabolites of both oxidation and reduction in HLS9 fractions (13.13 μl/min/mg protein), the Cl_{int} for the formation of SS-THBUP, RS-EHBUP, and SS-OHBUP accounted for 93.6%, 3.7%, and 2.8%, respectively. Compared with the total Cl_{int} (0.897 μl/min/mg protein) for the formation of R-BUP derived metabolites, the metabolic clearance of RR-THBUP, RR-OHBUP, and SR-EHBUP accounted for 71.3%, 14.9%, and 13.8%, respectively. The total metabolic clearance (Cl_{int}) of S-BUP derived metabolism by both oxidation and reduction was 14.7-fold higher than the total metabolic clearance via R-BUP metabolism. Thus, 93.6% of the total *in vitro* Cl_{int} of racemic BUP in pooled HLS9 fractions (oxidation + reduction) or hepatic Cl_{int} is due to S-BUP metabolism and 6.4% due to R-BUP metabolism, which was slightly higher or lower respectively

TABLE 2

Kinetic parameters for the stereoselective metabolism of BUP in cellular fractions of human liver

A range of concentrations of racemic BUP was incubated with cofactors and cellular fractions of human liver (0.4 mg protein/ml pooled HLMs and HLS9 fraction and 0.2 mg protein/ml HLCs) at 37°C for 20 min (see Materials and Methods). Formation rates of metabolites generated (SR-EHBUP, RS-EHBUP, RR-THBUP, SS-THBUP, RR-OHBUP, and SS-OHBUP) versus substrate concentrations were fit to the Michaelis-Menten equation to estimate kinetic parameters (V_{max} and K_m). Cl_{int} was calculated as the ratio of the V_{max} and K_m (V_{max}/K_m).

Substrate and Metabolites	Cellular Fraction	V_{max} (pmol /min/mg Protein)	K_m (μM)	Cl_{int} (μl/min/mg Protein)	$Cl_{int,\ Hep}$ (l/h)	Total Organ Clearance (l/h)	$F_{m,\ enantiomer}$[a]	F_m[b]
R-bupropion	HLMs							
SR-EHBUP		1.80	17.9	0.101	0.43	0.09	0.08	0.007
RR-THBUP		8.85	40.4	0.219	0.95	0.20	0.16	0.015
RR-OHBUP		43.11	42.5	1.015	4.38	0.92	0.76	0.071
Total R-bupropion					5.76			
S-bupropion								
RS-EHBUP		8.92	29.8	0.300	1.29	0.3	0.02	0.021
SS-THBUP		164.20	17.8	9.235	39.85	10	0.71	0.643
SS-OHBUP		147.8	42.3	3.492	15.06	3.8	0.27	0.243
Total S-bupropion					56.20			
R-bupropion	HLS9							
SR-EHBUP		1.46	11.8	0.124	1.62	0.34	0.14	0.009
RR-THBUP		19.03	29.8	0.639	8.35	1.75	0.71	0.045
RR-OHBUP		5.14	38.4	0.134	1.75	0.37	0.15	0.010
Total R-bupropion					11.71			
S-bupropion								
RS-EHBUP		7.40	15.4	0.482	6.28	1.58	0.037	0.034
SS-THBUP		166.3	13.5	12.282	160.98	39.5	0.94	0.876
SS-OHBUP		13.97	38.3	0.364	4.77	1.20	0.03	0.026
Total S-bupropion					172.02			
R-bupropion	HLCs							
SR-EHBUP		0.222	9.76	0.023	0.20	0.04	0.07	0.008
RR-THBUP		36.02	117.8	0.306	2.66	0.56	0.93	0.103
Total R-bupropion					2.86			
S-bupropion								
RS-EHBUP		4.66	57.6	0.081	0.71	0.2	0.03	0.028
SS-THBUP		23.53	9.23	2.55	22.2	5.6	0.97	0.861
Total S-bupropion					22.92			

[a]Fraction metabolized to each metabolite from respective individual bupropion enantiomer was calculated from $Cl_{int,\ Hep}$ for all subcellular fractions, HLMs, HLS9 fractions, and HLCs.
[b]Fraction metabolized to each metabolite from racemic bupropion was calculated from $Cl_{int,\ Hep}$ for all subcellular fractions, HLMs, HLS9 fractions, and HLCs.

than those values in HLMs. Formation clearance of BUP to THBUP (12.922 μl/min/mg protein), EHBUP (0.606 μl/min/mg protein), and OHBUP (0.498 μl/min/mg protein) accounted for 92.1%, 4.3%, and 3.6% of the total metabolic clearance of racemic BUP via both oxidation and hydroxylation, respectively. As described above, the formation clearance of RR- and SS-OHBUP and the predicted hepatic Cl_{int} was much lower in HLS9 fractions than in HLMs. However, the *in vitro* Cl_{int} for the formation of SR- EHBUP, RR-THBUP, RS-EHBUP, and SS-THBUP was slightly higher in HLS9 fractions (by 1.2-, 2.9-, 1.6-, and 1.3-fold, respectively), which was translated to 3.7-, 8.8-, 4.9-, 4.0-, and 3.1-fold higher predicted *in vivo* hepatic Cl_{int}, respectively (Table 2, middle panel).

As expected, 4-OHBUP was only detected when racemic or enantiomers of BUP were incubated with HLMs and HLS9 fractions but not in the other cellular fractions tested (HLCs, HIMs, and HICs). This data was a result of the lack or negligible expression of CYP2B6 in HLCs and cellular fractions of human intestine (Paine et al., 2006).

Pooled HLCs. To assess the contribution of cytosols to the overall liver metabolism, the stereoselective metabolism of BUP was determined in HLCs. Representative Michaelis-Menten kinetics of BUP reduction to diastereomers of THBUP and EHBUP in HLCs are shown in Fig. 5 and Table 2 (lower panel). As expected, SS- and RR-OHBUP were not detected in HLCs. Both THBUP and EHBUP were formed in HLCs to a variable extent. The V_{max} and Cl_{int} for the formation of SS-THBUP were 12.8- and 8.3-fold higher, respectively, than those of RR-THBUP; the K_m values were comparable. The extent of this stereoselectivity was somewhat lower than those observed in HLMs and HLS9 fractions. The K_m, V_{max}, and Cl_{int} for the formation of RS-EHBUP were 21-, 5.9-, and 3.6-fold higher than the values for the formation of SR-EHBUP (Table 2, lower panel), broadly consistent with the data in HLMs and HLS9 fractions. The total Cl_{int} for the formation of S-BUP derived reduction was 2.631 μl/min/mg protein (96.9% and 3.1% of this was due to formation of SS-THBUP and RS-EHBUP, respectively) and of R-BUP derived reduction was 0.329 μl/min/mg protein (with formation of RR-THBUP accounting for 93.1% and SR-EHBUP for 6.9%). Relative to the total Cl_{int} for the reduction of BUP to EHBUP and THBUP (2.96 μl/min/mg protein), reduction to THBUP (SS- and RR-THBUP) (2.86 μl/min/mg protein) accounted for ~96.5% and reduction to EHBUP (RS- and SR-EHBUP) (0.104 μl/min/mg protein) accounted for only 3.5%. Relative to the total metabolic clearance, the formation of SS-THBUP were the predominant metabolites in HLCs (86.2% of total) followed by RR-THBUP (10.3% of total), RS-EHBUP (2.7% of total), and SR-EHBUP (0.8% of total). Based on *in vitro* Cl_{int} (and predicted *in vivo* Cl_{int}), reduction of BUP (to THBUP and EHBUP) in pooled HLCs accounted for 23.1% (and 37.7%) of the total BUP reduction in pooled human liver (HLMs + HLCs) and 17.1% (and 29.4%) of the total metabolism of BUP (oxidation + reduction) occurred in HLCs.

Stereoselective Metabolism of BUP in HIMs, HIS9 Fractions, and HICs

Stereospecific metabolism of BUP was tested in cellular fractions derived from human intestine.

Pooled HIMs. The kinetics for the stereoselective metabolism of BUP were determined in pooled HIMs and show that BUP is efficiently and exclusively converted to RR-THBUP, as shown by the lower K_m (2.6-fold) and substantially higher V_{max} (>162-fold) and Cl_{int}

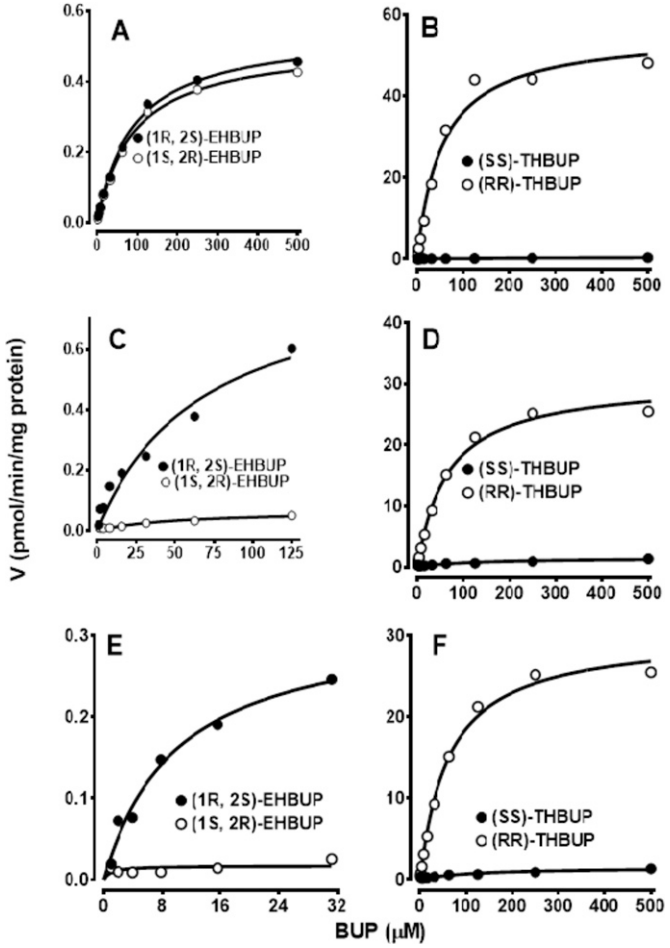

Fig. 6. Stereoselective metabolism of BUP in HIMs, HIS9 fractions, and HICs. Increasing concentrations of racemic BUP (1.96–4000 μM) consisting of 50%/50% of R- and S-BUP were incubated in duplicate with cellular fractions of human intestine (0.4 mg protein/ml pooled HIMs or 0.2 mg protein/ml HIS9 fractions and HICs) for 20 minutes at 37°C. Formation rates of diastereomers of THBUP and EHBUP versus BUP concentrations (0.98–500 μM corresponding to R- and S-BUP) were fit to a Michaelis Menten equation. Formation rates of BUP metabolites in HIMs (A and B), HIS9 fractions (C and D), and HICs (E and F) are shown. Each point represents an average of duplicate incubations. Corresponding kinetic parameters derived from fitting the formation rate of metabolite (V) versus substrate concentration to the Michaelis-Menten equation using a nonlinear regression analysis in GraphPad Prism 7 (Version 7.01, San Diego, CA; www.graphpad.com) are listed in Table 3.

(>400-fold) compared with the formation of SS-THBUP (Fig. 6 and Table 3, upper panel). Reduction of BUP to RR-THBUP accounted for 98.5% of total reduction in HIMs; the formation of SS-THBUP accounted for only 0.24%. Although formation of RS- and SR-EHBUP was also detected at a comparable metabolic clearance rate (nonstereospecific), these routes only accounted for a small fraction (0.64% and 0.59%, respectively) of the total Cl_{int} in HIMs. Metabolism of BUP to THBUP was the major route in HIMs (98.8% of total reduction). The contribution of BUP metabolism to EHBUP was minor (1.2%). Reduction of BUP in HIMs was 14.9-fold lower than in HLMs and accounts for only 6.3% of total (HLMs and HIMs) and 8.9% of the total reduction (HLMs + HIMs). These values were lower (1.5% and 2.3%, respectively) when the contribution was calculated based on the predicted *in vivo* hepatic Cl_{int}.

Pooled HIS9 Fractions. The stereoselective metabolism of BUP in HIS9 fractions is shown in Fig. 6 and Table 3 (middle panels). The total Cl_{int} in HIS9 fractions (0.493 μl/min/mg protein) was smaller by 49% than the total Cl_{int} in HIMs (0.961 μl/min/mg protein). The total Cl_{int} in HIS9 fractions was 28.5-fold lower than the values in HLS9 fractions and accounts for 3.4% and 3.5% of the total oxidation and reduction of BUP (HLS9 and HIS9 fractions) or reduction of BUP (HLS9 and HIS9 fractions), respectively. As with the data in HIMs, marked stereoselectivity was noted with respect to the formation of diastereomers of THBUP: the formation clearance of RR-THBUP in HIS9 fractions was much higher (~20- and 36.7-fold higher V_{max} and Cl_{int}, respectively) compared with the formation of SS-THBUP. In contrast to those data in HIMs, the formation clearance of RS- EHBUP was much higher (13.2- and 9.6-fold higher V_{max} and Cl_{int}, respectively) compared with that of SR-EHBUP, indicating marked stereoselectivity in HIS9 fractions (but not in HIMs). The formation of RR-THBUP, RS-EHBUP, SS-THBUP, and SR-EHBUP accounted for 94.5%, 2.6%, 2.6%, and 0.28% of the total Cl_{int} in HIS9 fractions, respectively (97.1% THBUP and 2.9% EHBUP of total).

Pooled HICs. Stereoselective metabolism of BUP was determined in HICs. As shown in Fig. 6 and Table 3 (lower panels), the formation of RS-EHBUP was 9.6-fold higher than the V_{max} of SR-EHBUP. The K_m, $V_{max,}$ and Cl_{int} of RR-THBUP formation from BUP was 9.4-fold lower and 14.1 and 133.2-fold higher, respectively, than the formation of SS-THBUP. The contribution of the formation of RR-THBUP, RS-EHBUP, SS-THBUP, and SR-EHBUP to the overall reduction in HICs was 94.9%, 3.8%, 0.7%, and 0.5%, respectively. Relative to the total Cl_{int} for the formation of EHBUP and THBUP in pooled HICs (0.281 μl/min/mg protein), reduction to THBUP (SS- and RR-THBUP) (0.269 μl/min/mg protein) accounted for ~95.7%, and reduction to EHBUP (RS- and SR-EHBUP) (0.012 μl/min/mg protein) accounted for only 4.3%. The summation of Cl_{int} in HIMs (0.961 μl/min/mg protein) and HICs (0.281 μl/min/mg protein) was 1.422 μl/min/mg protein, i.e., 77.4% and 22.6% of the total intestinal reduction of BUP occurred in HIMs and HICs, respectively. In addition, approximately 6.7% of the total BUP metabolism (oxidation + reduction) occurs in the intestine (HIMs and HICs), whereas 93.3% occurs in the liver (HLMs + HLCs); ~10% of total BUP reduction occurs in the intestine (HIM + HICs) and 90% in human liver (HLMs + HLCs).

Metabolic Profiles of S-BUP in Cellular Fractions of Human Intestine

The unique observation that RR-THBUP was quantitatively the sole metabolite formed from racemic BUP in cellular fractions of human intestine prompted use to closely analyze the kinetics for the metabolism of S-BUP, which was already run in parallel to that of racemic BUP as a positive internal control in all human intestine and liver cellular fractions. Diastereomers of THBUP formed from S-BUP were quantified after chiral separation as described in the *Methods* section. As shown in Fig. 7 and Table 4, S-BUP was efficiently converted to RR-THBUP in all cellular fractions of human intestine tested, whereas its metabolism to SS-THBUP was negligible. These data are in sharp contrast to those observed in cellular fractions of human liver, where SS-THBUP was by far the major metabolite formed from S-BUP.

Discussion

In this study, *in vitro* stereospecific metabolism of BUP was characterized in cellular fractions of human liver and intestine. Our data provide the first detailed information on BUP racemization. We demonstrated striking stereoselective reduction of BUP in HLCs, HIMs, HIS9 fractions, and HICs for the first time. We have confirmed and further expanded stereoselective reduction and 4-hydroxylation of BUP in HLMs and HLS9 fractions. These data provide new and quantitative insight into tissue- and tissue fraction- dependent stereoselective

TABLE 3

Kinetic parameters for the stereoselective metabolism of BUP in cellular fractions of human intestine

A range of concentrations of racemic BUP was incubated with cofactors and cellular fractions of human intestine (0.4 mg protein/ml pooled HIMs and 0.2 mg protein/ml HIS9 fraction and HICs) at 37°C for 20 min (see Materials and Methods). Formation rates of metabolites generated (SR-EHBUP, RS-EHBUP, RR-THBUP, and SS-THBUP) versus substrate concentrations were fit to the Michaelis-Menten equation to estimate kinetic parameters (V_{max} and K_m). Cl_{int} was calculated as the ratio of the V_{max} and K_m (V_{max}/K_m).

Substrate and Metabolites	Cellular Fraction	V_{max} (pmol/min/mg Protein)	K_m (μM)	Cl_{int} (μl/min/mg Protein)	$Cl_{int,\ Intes}$ (l/h)	Total Organ Clearance (l/h)	$F_{m,\ enantiomer}$ [a]	F_m [b]
R-bupropion	HIMs							
SR-EHBUP		0.51	89.4	0.0057	0.0057	0.0012	0.0060	0.006
RR-THBUP		59.48	62.8	0.947	0.95	0.20	0.94	0.985
Total R-bupropion					0.956			
S-bupropion								
RS-EHBUP		0.55	89.5	0.0061	0.0061	0.00155	0.73	0.006
SS-THBUP		0.366	161.8	0.0023	0.0023	0.00057	0.27	0.002
Total S-bupropion					0.0084			
R-bupropion	HIS9							
SR-EHBUP		0.067	49.6	0.0014	0.0025	0.001	0.003	0.003
RR-THBUP		30.68	65.9	0.466	0.87	0.183	0.997	0.945
Total R-bupropion					0.873			
S-bupropion								
RS-EHBUP		0.89	68.2	0.0130	0.0245	0.00616	0.51	0.027
SS-THBUP		1.54	121.1	0.0127	0.0238	0.00600	0.49	0.026
Total S-bupropion					0.0483			
R-bupropion	HICs							
SR-EHBUP		0.147	101.7	0.0014	0.001	0.00027	0.01	0.004
RR-THBUP		13.6	51.1	0.267	0.23	0.049	0.99	0.949
Total R-bupropion					0.231			
S-bupropion								
RS-EHBUP		1.404	130.3	0.0108	0.00941	0.00237	0.84	0.039
SS-THBUP		0.97	483	0.002	0.002	0.00044	0.16	0.008
Total S-bupropion					0.0114			

[a]Fraction metabolized to each metabolite from respective individual bupropion enantiomer was calculated from $Cl_{int,\ Intes}$ for all subcellular fractions, HIMs, HIS9 fractions, and HICs.
[b]Fraction metabolized to each metabolite from racemic bupropion was calculated from $Cl_{int,\ Intes}$ for all subcellular fractions, HIMs, HIS9 fractions, and HICs.

metabolism of BUP and may offer mechanistic explanations for the marked stereospecific disposition of BUP observed clinically.

Our data show that both R- and S-BUP racemize effectively during incubation with pooled HLMs (Fig. 3), consistent with findings in literature (Fang et al., 2000). In HLMs, the total Cl_{int} for the formation of S- and R-BUP derived metabolites accounted for 90.7% and 9.3% of the total racemic BUP metabolism. Metabolic formation clearance of SS-THBUP was higher (over 8-fold) than that of RR-THBUP. The efficient conversion of R-BUP to S-BUP derived metabolites was therefore dictated by a much higher rate of metabolism of S-BUP in HLMs than by the differences in racemization of R- to S-BUP and vice versa. This suggestion is further supported by the data derived from cellular fractions of human intestine, where RR-THBUP was formed at the highest rate whether R- or S-BUP was incubated (Fig. 7; Table 4). Together, for enantiomers showing chiral inversion, measurement of both metabolites formed and substrates in the incubations using a chiral assay are needed before deciding to use individual enantiomers for stereoselective metabolism studies.

Our data showing efficient BUP reduction to THBUP and EHBUP and oxidation to OHBUP in HLMs and HLS9 fractions concurs with published reports (Faucette et al., 2000; Coles and Kharasch, 2008; Molnari and Myers, 2012; Meyer et al., 2013; Skarydova et al., 2014;

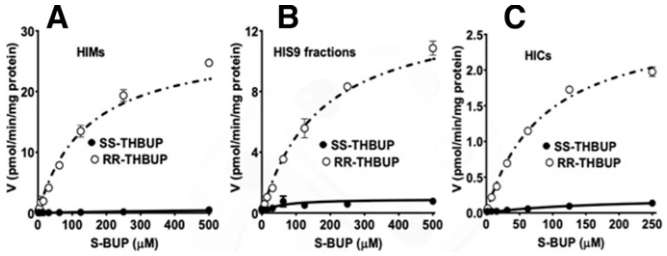

Fig. 7. Metabolism of S-BUP in cellular fractions of human intestine. Increasing concentrations of S-BUP were incubated in duplicate with cellular fractions of human intestine (0.4 mg protein/ml pooled HIMs and 0.2 mg protein/ml HIS9 fractions and HICs) for 20 minutes at 37°C. Diastereomers of THBUP monitored using a chiral assay. Formation rates of SS- and RR-THBUP versus substrate (S-BUP) concentrations were fit to the Michalis-Menten equation: (A) HIMs, (B) HIS9 fractions, and (C) HICs. Each point represents an average of duplicate incubations. Corresponding kinetic parameters derived from fitting the formation rate of metabolite (V) versus substrate concentration to the Michaelis-Menten equation using a nonlinear regression analysis in GraphPad Prism 7 (Version 7.01, San Diego, CA; www.graphpad.com) are listed in Table 4.

TABLE 4

Metabolism of S-BUP in cellular fractions of human intestine

Increasing concentrations of S-BUP were incubated in duplicate with cellular fractions of human intestine (0.4 mg protein/ml pooled HIMs and 0.2 mg protein/ml HIS9 fraction and HICs) for 20 min at 37°C. Diastereomers of THBUP monitored using a chiral assay. Kinetic parameters derived from fitting the formation rate of metabolite (V) versus substrate concentration to the Michaelis-Menten equation using a nonlinear regression analysis in GraphPad Prism 7 (Version 7.01, San Diego, CA; www.graphpad.com).

	V_{max} (pmol/min/mg Protein)	K_m (μM)	Cl_{int} (μl/min/mg Protein)	Cl_{int} RR-/SS-THBUP
HIMs:				
SS-THBUP	1.19	955	0.0012	
RR-THBUP	28.27	140.8	0.201	162
HIS9 Fractions:				
SS-THBUP	0.928	47.2	0.0197	
RR-THBUP	13.61	171.5	0.0794	4.0
HICs:				
SS-THBUP	0.223	164.4	0.0014	
RR-THBUP	2.74	86.4	0.0317	23.4

Connarn et al., 2015; Sager et al., 2016). Except in HLMs and HLS9 fractions, no OHBUP was detected in HLCs and any of the cellular fractions of human intestine, consistent with the lack (HLCs) or negligible expression of CYP2B6 in human intestine (Paine et al., 2006). BUP 4-hydroxylation is an important bioactivation pathway and a marker of CYP2B6 activity, but the fraction metabolized via 4-hydroxylation is small. This is supported by the lack of meaningful effects of CYP2B6 strong inhibitors (Palovaara et al., 2003; Turpeinen et al., 2005) or slow metabolizers of CYP2B6 (Eum et al., 2022) on BUP systemic clearance. The present findings and recent data (Sager et al., 2016) suggest that BUP reduction to THBUP represents the major clearance mechanism of BUP in human liver. It follows that BUP systemic clearance is likely altered more significantly via modulation of the reduction pathways than 4-hydroxylation.

Our data are the first to demonstrate stereoselective reduction of BUP in HLCs and cellular fractions of human intestine. 1) In HLCs, we estimate that reduction accounts for 37.7% and 29.4% of the total predicted *in vitro* hepatic Cl_{int} of human liver reduction and oxidation + reduction, respectively. Marked stereospecific reduction favoring a higher rate of metabolism to S-BUP derived metabolites (RS-EHBUP by over 3-fold and SS-THBUP by over 8-fold) than the respective R-derived metabolites was noted. This difference was mainly dictated by the 12.8-fold lower K_m and ~21-fold higher V_{max} for the formation of SS-THBUP and RS-EHBUP than those of RR-THBUP and SR-EHBUP, respectively. These data are the first stereoselective reductions of BUP in HLCs and provide insight into stereoselective enzyme-substrate binding and turnover number of the enzymes involved. 2) Our kinetic data in cellular fractions of human intestine demonstrated striking stereoselective reduction of BUP to THBUP, where metabolic formation clearance to RR-THBUP accounted for over 95% of total BUP reduction in each cellular fraction (HIMs, HIS9 fractions, and HICs). The contribution of metabolic formation clearance to SS-THBUP was marginal. Although racemic EHBUP was undetected in incubation of BUP with cellular fractions of human intestine in a previous study (Connarn et al., 2015), we were able to detect and characterize SR- and RS-EHBUP and SS-THBUP in all cellular fractions of human intestine in this study, probably due to higher sensitivity of our UHPLC/MS/MS method. Our data suggest nonstereoselective reduction of BUP to RS- and SR-EHBUP in HIMs, although marked stereoselective reduction (higher Cl_{int} of RS-EHBUP) in HIS9 fractions and HICs was noted, implying different enzymes may be involved in HIMs versus HICs. However, the contribution of BUP reduction to EHBUP combined with the formation of SS-THBUP (aggregate Cl_{int} of RS- and SR-EHBUP and SS-THBUP) is negligible ($\leq$ 5%). Together, the present data demonstrated for the first time marked stereoselectivity in all cellular fractions of human intestine, and further confirm and expand the notion that BUP reduction occurs in these cellular fractions.

Our data suggest HLMs is likely more appropriate to quantitatively estimate CYP-mediated oxidative catalytic efficiency because the Cl_{int} of both SS- and RR-OHBUP in HLS9 fractions was lower (>7-fold) than in HLMs, probably due to lower CYP amount/activity in HLS9 fractions than in HLMs (Jia and Liu, 2007). Despite this, the Cl_{int} for the formation of SS-OHBUP was greater (by 3.3-fold) compared with that of RR-OHBUP in both HLMs and HLS9 fractions, consistent with previous reports (Coles and Kharasch, 2008; Sager et al., 2016; Wang et al., 2020). CYP2B6 exclusively catalyzes 4-hydroxylation of racemic BUP and its enantiomers *in vitro* (Faucette et al., 2000; Coles and Kharasch, 2008) and *in vivo* (Benowitz et al., 2013; Kharasch and Crafford, 2019). However, the extent of stereoselectivity observed in the present study and the literature cannot fully explain the marked difference in the disposition of SS- versus RR-OHBUP observed clinically (Masters et al., 2016a; Kharasch et al., 2020), suggesting mechanisms other than CYP2B6 [e.g., subsequent metabolism (Gufford et al., 2016) or renal excretion (Masters et al., 2016a)] of SS- versus RR-OHBUP may explain clinically observed disposition of OHBUP diastereomers. Higher Cl_{int} for the reduction of BUP to SS-THBUP (42.1- and 19.2-fold) was observed in HLMs and HLS9 fractions, respectively, compared with the Cl_{int} for the formation of RR-THBUP. The extent of stereoselectivity was smaller (<14-fold) in previous reports from HLMs and HLS9 fractions (Sager et al., 2016; Bhattacharya et al., 2019). This discrepancy is likely due to differences in study design and procedures used to estimate the kinetic parameters. Our kinetic experiments were performed using racemic BUP as a substrate, the metabolites formed were quantified after chiral separation, and kinetic parameters (V_{max} and K_m) were estimated from saturable substrate concentration range in contrast to the other studies using R- and S-BUP as substrates, achiral column to quantify the metabolites formed, and estimation of Cl_{int} from the initial slope of the formation rate (V) versus substrate concentration (S) plots. Approximately a 3-fold higher Cl_{int} for the formation of RS-EHBUP than that of SR-EHBUP in HLMs and HLS9 fractions observed in the present study concurs with the previous findings (Sager et al., 2016; Bhattacharya et al., 2019).

The marked difference in stereoselective metabolism among human liver and intestine and between cellular fractions is intriguing. Skarydova et al. (2014) identified four cytosolic carbonyl-reductase enzymes (AKR1C1, AKR1C2, AKR1C3, and CBR1) and one microsomal carbonyl reductase enzyme, 11β -HSD, involved in the reduction of BUP to THBUP and EHBUP. Since enzymes catalyzing stereoselective BUP reduction in any of the tissues and cellular fractions have not been so far identified, the specific contribution of these or other enzymes in the stereoselective reduction of BUP remains to be determined. However, useful information can be gleaned from the present data and published literature that allow speculation of which major enzymes may be involved. Inhibition studies (Molnari and Myers, 2012; Meyer et al., 2013; Connarn et al., 2015) suggest that the carbonyl reduction of racemic BUP to THBUP and EHBUP in HLMs is mainly catalyzed by 11β-HSD1 and in HLCs by AKRs. These data are further supported by experiments in recombinant enzymes showing that 11β -HSD1 and AKRs (e.g., AKR1C1) catalyze BUP reduction to THBUP and EHBUP at the highest rate (Skarydova et al., 2014). The microsomal enzyme, 11β-HSD1, is abundantly expressed in HLMs with no expression detected in HIMs (Connarn et al., 2015; Yang et al., 2018). Our data indicate that reduction of BUP to SS-THBUP quantitatively was the major pathway in human liver, whereas this was the reverse in human intestine, where the formation of RR-THBUP was predominant. Thus, we speculate that 11β-HSD1 is responsible for the reduction of S-BUP to SS-THBUP in HLMs, and the reduction of R-BUP to RR-THBUP in the intestine appears to occur via enzymes other than 11β-HSD1. This suggestion is consistent with the lack (or marginal) formation of SS-THBUP in cellular fractions of intestine and with published data showing that specific inhibitors of 11β-HSD1 had no effect on the formation of racemic THBUP in cellular fractions of human intestine, whereas flufenamic acid (AKR family inhibitor) reduced the formation of THBUP by 57.8% to 78.7% (Connarn et al., 2015). Together, these data suggest that AKRs may be important BUP reductase in human intestine. Whether these AKRs may also catalyze BUP reduction to RR-THBUP in HLMs remains to be determined. Based on molecular docking data, 11β-HSD1 was predicted to selectively convert R-BUP to THBUP in HLMs, but this prediction lacks experimental verification (Meyer et al., 2013) and is not supported by the present data. Unlike the differential formation of SS- and RR-THBUP in human liver and intestine, stereoselective reduction of BUP to EHBUP was in favor of S-BUP reduction to RS-EHBUP in both cellular

fractions of human liver and intestine except in HIMs, which showed no stereoselectivity. Based on these data, it is conceivable that 11β-HSD1 may be dominant for the formation of RS-EHBUP in HLMs; other microsomal enzymes could be important for the formation of SR-EHBUP in HLMs and for SR- and RS-EHBUP formation in HIMs; and AKRs appear to catalyze BUP reduction in cytosols of human liver and intestine. According to Meyer et al. (2013), the existence of enzymes other than 11β-HSD1 that generates EHBUP from BUP in HLMs was suggested. Together, since HLMs is the major site of BUP reduction and 11β-HSD1 appears to play a major role in this cellular fraction, further detailed *in vitro* investigation would be required to address which specific enzyme catalyzes the formation of diastereomers of THBUP and EHBUP and their contribution in each of the cellular fractions tested.

In summary, S-BUP is metabolized at the highest rate, particularly to SS-THBUP, than R-BUP in cellular fractions of human liver, whereas over 95% of total reduction in cellular fractions of human intestine is due to R-BUP metabolism to RR-THBUP. Although HLMs remain the major cellular fraction involved in the stereoselective metabolism of BUP, HLCs and intestinal fractions also contribute to variable extent. These novel data provide the critical first step to understand interpatient variability in the disposition, effects, and CYP2D6-mediated DDI of BUP.

Authorship Contributions

Participated in research design: Lu, Desta.
Conducted experiments: Bamfo, Lu.
Performed data analysis: Bamfo, Lu, Desta.
Wrote or contributed to the writing of the manuscript: Bamfo, Lu, Desta.

References

Ascher JA, Cole JO, Colin JN, Feighner JP, Ferris RM, Fibiger HC, Golden RN, Martin P, Potter WZ, Richelson E, et al. (1995) Bupropion: a review of its mechanism of antidepressant activity. *J Clin Psychiatry* **56**:395–401.

Benowitz NL, Zhu AZ, Tyndale RF, Dempsey D, and Jacob 3rd P (2013) Influence of CYP2B6 genetic variants on plasma and urine concentrations of bupropion and metabolites at steady state. *Pharmacogenet Genomics* **23**:135–141.

Bhattacharya C, Kirby D, Van Stipdonk M, and Stratford RE (2019) Comparison of *in vitro* stereoselective metabolism of bupropion in human, monkey, rat, and mouse liver microsomes. *Eur J Drug Metab Pharmacokinet* **44**:261–274.

Carroll FI, Blough BE, Mascarella SW, Navarro HA, Lukas RJ, and Damaj MI (2014) Bupropion and bupropion analogs as treatments for CNS disorders. *Adv Pharmacol* **69**:177–216.

Coles R and Kharasch ED (2008) Stereoselective metabolism of bupropion by cytochrome P4502B6 (CYP2B6) and human liver microsomes. *Pharm Res* **25**:1405–1411.

Connarn JN, Zhang X, Babiskin A, and Sun D (2015) Metabolism of bupropion by carbonyl reductases in liver and intestine. *Drug Metab Dispos* **43**:1019–1027.

Costa R, Oliveira NG, and Dinis-Oliveira RJ (2019) Pharmacokinetic and pharmacodynamic of bupropion: integrative overview of relevant clinical and forensic aspects. *Drug Metab Rev* **51**:293–313.

Cubitt HE, Houston JB, and Galetin A (2009) Relative importance of intestinal and hepatic glucuronidation-impact on the prediction of drug clearance. *Pharm Res* **26**:1073–1083.

Cubitt HE, Houston JB, and Galetin A (2011) Prediction of human drug clearance by multiple metabolic pathways: integration of hepatic and intestinal microsomal and cytosolic data. *Drug Metab Dispos* **39**:864–873.

Damaj MI, Carroll FI, Eaton JB, Navarro HA, Blough BE, Mirza S, Lukas RJ, and Martin BR (2004) Enantioselective effects of hydroxy metabolites of bupropion on behavior and on function of monoamine transporters and nicotinic receptors. *Mol Pharmacol* **66**:675–682.

Dash RP, Rais R, and Srinivas NR (2018) Chirality and neuropsychiatric drugs: an update on stereoselective disposition and clinical pharmacokinetics of bupropion. *Xenobiotica* **48**:945–957.

Davidson J (1989) Seizures and bupropion: a review. *J Clin Psychiatry* **50**:256–261.

Davies B and Morris T (1993) Physiological parameters in laboratory animals and humans. *Pharm Res* **10**:1093–1095.

Daviss WB, Perel JM, Rudolph GR, Axelson DA, Gilchrist R, Nuss S, Birmaher B, and Brent DA (2005) Steady-state pharmacokinetics of bupropion SR in juvenile patients. *J Am Acad Child Adolesc Psychiatry* **44**:349–357.

Dwoskin LP, Rauhut AS, King-Pospisil KA, and Bardo MT (2006) Review of the pharmacology and clinical profile of bupropion, an antidepressant and tobacco use cessation agent. *CNS Drug Rev* **12**:178–207.

Eum S, Sayre F, Lee AM, Stingl JC, and Bishop JR (2022) Association of CYP2B6 genetic polymorphisms with bupropion and hydroxybupropion exposure: a systematic review and meta-analysis. *Pharmacotherapy* **42**:34–44.

Fang QK, Han Z, Grover P, Kessler D, Senanayake CH, and Wald S (2000) Rapid access to enantiopure bupropion and its major metabolite by stereospecific nucleophilic substitution on an α-ketotriflate. *Tetrahedron Asymmetry* **11**:3659–3663.

Faucette SR, Hawke RL, Lecluyse EL, Shord SS, Yan B, Laethem RM, and Lindley CM (2000) Validation of bupropion hydroxylation as a selective marker of human cytochrome P450 2B6 catalytic activity. *Drug Metab Dispos* **28**:1222–1230.

Foley KF, DeSanty KP, and Kast RE (2006) Bupropion: pharmacology and therapeutic applications. *Expert Rev Neurother* **6**:1249–1265.

Fryer JD and Lukas RJ (1999) Noncompetitive functional inhibition at diverse, human nicotinic acetylcholine receptor subtypes by bupropion, phencyclidine, and ibogaine. *J Pharmacol Exp Ther* **288**:88–92.

Gheldiu AM, Popa A, Neag M, Muntean D, Bocsan C, Buzoianu A, Vlase L, Tomuta I, and Briciu C (2016) Assessment of a potential pharmacokinetic interaction between nebivolol and bupropion in healthy volunteers. *Pharmacology* **98**:190–198.

Gufford BT, Lu JB, Metzger IF, Jones DR, and Desta Z (2016) Stereoselective glucuronidation of bupropion metabolites *in vitro* and *in vivo Drug Metab Dispos* **44**:544–553.

Hesse LM, Venkatakrishnan K, Court MH, von Moltke LL, Duan SX, Shader RI, and Greenblatt DJ (2000) CYP2B6 mediates the *in vitro* hydroxylation of bupropion: potential drug interactions with other antidepressants. *Drug Metab Dispos* **28**:1176–1183.

Hurt RD, Sachs DP, Glover ED, Offord KP, Johnston JA, Dale LC, Khayrallah MA, Schroeder DR, Glover PN, Sullivan CR, et al. (1997) A comparison of sustained-release bupropion and placebo for smoking cessation. *N Engl J Med* **337**:1195–1202.

Irvine JD, Takahashi L, Lockhart K, Cheong J, Tolan JW, Selick HE, and Grove JR (1999) MDCK (Madin-Darby canine kidney) cells: a tool for membrane permeability screening. *J Pharm Sci* **88**:28–33.

Jefferson JW, Pradko JF, and Muir KT (2005) Bupropion for major depressive disorder: pharmacokinetic and formulation considerations. *Clin Ther* **27**:1685–1695.

Jia L and Liu X (2007) The conduct of drug metabolism studies considered good practice (II): *in vitro* experiments. *Curr Drug Metab* **8**:822–829.

Johnston JA, Fiedler-Kelly J, Glover ED, Sachs DP, Grasela TH, and DeVeaugh-Geiss J (2001) Relationship between drug exposure and the efficacy and safety of bupropion sustained release for smoking cessation. *Nicotine Tob Res* **3**:131–140.

Kharasch ED and Crafford A (2019) Common polymorphisms of CYP2B6 influence stereoselective bupropion disposition. *Clin Pharmacol Ther* **105**:142–152.

Kharasch ED, Neiner A, Kraus K, Blood J, Stevens A, Miller JP, and Lenze EJ (2020) Stereoselective steady-state disposition and bioequivalence of brand and generic bupropion in adults. *Clin Pharmacol Ther* **108**:1036–1048.

Kotlyar M, Brauer LH, Tracy TS, Hatsukami DK, Harris J, Bronars CA, and Adson DE (2005) Inhibition of CYP2D6 activity by bupropion. *J Clin Psychopharmacol* **25**:226–229.

Laib AK, Brünen S, Pfeifer P, Vincent P, and Hiemke C (2014) Serum concentrations of hydroxybupropion for dose optimization of depressed patients treated with bupropion. *Ther Drug Monit* **36**:473–479.

Masters AR, Gufford BT, Lu JB, Metzger IF, Jones DR, and Desta Z (2016a) Chiral plasma pharmacokinetics and urinary excretion of bupropion and metabolites in healthy volunteers. *J Pharmacol Exp Ther* **358**:230–238.

Masters AR, McCoy M, Jones DR, and Desta Z (2016b) Stereoselective method to quantify bupropion and its three major metabolites, hydroxybupropion, erythro-dihydrobupropion, and threo-dihydrobupropion using HPLC-MS/MS. *J Chromatogr B Analyt Technol Biomed Life Sci* **1015-1016**:201–208.

Meyer A, Vuorinen A, Zielinska AE, Strajhar P, Lavery GG, Schuster D, and Odermatt A (2013) Formation of threohydrobupropion from bupropion is dependent on 11β-hydroxysteroid dehydrogenase 1. *Drug Metab Dispos* **41**:1671–1678.

Molnari JC and Myers AL (2012) Carbonyl reduction of bupropion in human liver. *Xenobiotica* **42**:550–561.

Nishimuta H, Houston JB, and Galetin A (2014) Hepatic, intestinal, renal, and plasma hydrolysis of prodrugs in human, cynomolgus monkey, dog, and rat: implications for *in vitro-in vivo* extrapolation of clearance of prodrugs. *Drug Metab Dispos* **42**:1522–1531.

Paine MF, Hart HL, Ludington SS, Haining RL, Rettie AE, and Zeldin DC (2006) The human intestinal cytochrome P450 "pie". *Drug Metab Dispos* **34**:880–886.

Paine MF, Khalighi M, Fisher JM, Shen DD, Kunze KL, Marsh CL, Perkins JD, and Thummel KE (1997) Characterization of interintestinal and intraintestinal variations in human CYP3A-dependent metabolism. *J Pharmacol Exp Ther* **283**:1552–1562.

Palovaara S, Pelkonen O, Uusitalo J, Lundgren S, and Laine K (2003) Inhibition of cytochrome P450 2B6 activity by hormone replacement therapy and oral contraceptive as measured by bupropion hydroxylation. *Clin Pharmacol Ther* **74**:326–333.

Pandhare A, Pappu AS, Wilms H, Blanton MP, and Jansen M (2017) The antidepressant bupropion is a negative allosteric modulator of serotonin type 3A receptors. *Neuropharmacology* **113** (Pt A):89–99.

Petsalo A, Turpeinen M, and Tolonen A (2007) Identification of bupropion urinary metabolites by liquid chromatography/mass spectrometry. *Rapid Commun Mass Spectrom* **21**:2547–2554.

Reese MJ, Wurm RM, Muir KT, Generaux GT, St John-Williams L, and McConn DJ (2008) An *in vitro* mechanistic study to elucidate the desipramine/bupropion clinical drug-drug interaction. *Drug Metab Dispos* **36**:1198–1201.

Sager JE, Price LS, and Isoherranen N (2016) Stereoselective metabolism of bupropion to OH-bupropion, threohydrobupropion, erythrohydrobupropion, and 4′-OH-bupropion *in vitro*. *Drug Metab Dispos* **44**:1709–1719.

Sager JE, Tripathy S, Price LS, Nath A, Chang J, Stephenson-Famy A, and Isoherranen N (2017) *In vitro* to in vivo extrapolation of the complex drug-drug interaction of bupropion and its metabolites with CYP2D6; simultaneous reversible inhibition and CYP2D6 downregulation. *Biochem Pharmacol* **123**:85–96.

Schroeder DH (1983) Metabolism and kinetics of bupropion. *J Clin Psychiatry* **44**:79–81.

Silverstone PH, Williams R, McMahon L, Fleming R, and Fogarty S (2008) Convulsive liability of bupropion hydrochloride metabolites in Swiss albino mice. *Ann Gen Psychiatry* **7**:19.

Skarydova L, Tomanova R, Havlikova L, Stambergova H, Solich P, and Wsol V (2014) Deeper insight into the reducing biotransformation of bupropion in the human liver. *Drug Metab Pharmacokinet* **29**:177–184.

Soroko FE, Mehta NB, Maxwell RA, Ferris RM, and Schroeder DH (1977) Bupropion hydrochloride ((+/-) alpha-t-butylamino-3-chloropropiophenone HCl): a novel antidepressant agent. *J Pharm Pharmacol* **29**:767–770.

Tanaudommongkon GBI, Lu J, and Desta Z (2019) CYP2D6 inhibition by bupropion and its metabolites is stereospecific and circulating metabolites accurately predict clinical bupropion-CYP2D6 interaction. *Clin Pharmacol Ther* **105**:(Suppl. 1); S113 (abstract # PIII-111).

Thase ME, Haight BR, Richard N, Rockett CB, Mitton M, Modell JG, VanMeter S, Harriett AE, and Wang Y (2005) Remission rates following antidepressant therapy with bupropion or selective serotonin reuptake inhibitors: a meta-analysis of original data from 7 randomized controlled trials. *J Clin Psychiatry* **66**:974–981.

Todor I, Popa A, Neag M, Muntean D, Bocsan C, Buzoianu A, Vlase L, Gheldiu AM, and Briciu C (2016) Evaluation of a potential metabolism-mediated drug-drug interaction between atomoxetine and bupropion in healthy volunteers. *J Pharm Pharm Sci* **19**:198–207.

Turpeinen M, Tolonen A, Uusitalo J, Jalonen J, Pelkonen O, and Laine K (2005) Effect of clopidogrel and ticlopidine on cytochrome P450 2B6 activity as measured by bupropion hydroxylation. *Clin Pharmacol Ther* **77**:553–559.

Wang X, He B, Shi J, Li Q, and Zhu HJ (2020) Comparative proteomics analysis of human liver microsomes and S9 fractions. *Drug Metab Dispos* **48**:31–40.

Welch RM, Lai AA, and Schroeder DH (1987) Pharmacological significance of the species differences in bupropion metabolism. *Xenobiotica* **17**:287–298.

Yang X, Hua W, Ryu S, Yates P, Chang C, Zhang H, and Di L (2018) 11β-Hydroxysteroid Dehydrogenase 1 human tissue distribution, selective inhibitor, and role in doxorubicin metabolism. *Drug Metab Dispos* **46**:1023–1029.

Yanovski SZ and Yanovski JA (2015) Naltrexone extended-release plus bupropion extended-release for treatment of obesity. *JAMA* **313**:1213–1214.

Zhu AZ, Cox LS, Nollen N, Faseru B, Okuyemi KS, Ahluwalia JS, Benowitz NL, and Tyndale RF (2012) CYP2B6 and bupropion's smoking-cessation pharmacology: the role of hydroxybupropion. *Clin Pharmacol Ther* **92**:771–777.

Address correspondence to: Dr. Zeruesenay Desta, Division of Clinical Pharmacology, Indiana University School of Medicine, 950 W Walnut Street, Research II Building, E425, Indianapolis, IN 46202. E-mail: zdesta@iu.edu

Drug Metabolism and Disposition

Manuscript # DMD-AR-2022-000867R1

Supplemental Files

Title: Stereoselective metabolism of bupropion to active metabolites in cellular fractions of human liver and intestine.

Authors: Nadia O Bamfo, Jessica Bo Li Lu, Zeruesenay Desta

Supplemental Table 1. Mass spectrometry conditions

MRM							
Compound	**Q1**	**Q3**	**Time (msec)**	**DP**	**EP**	**CE**	**CXP**
R- and S-BUP	240.0	184.0	10	40	10	17	21
RR- and SS-OHBUP	256.0	238.0	30	40	10	17	21
RS- and SR-EHBUP; RR-and SS-THBUP	242.0	168.0	30	35	10	26	20
Nevirapine (IS)	267.5	226.1	30	61	10	35	16

MS3								
Compound	**1st precursor**	**2nd precursor**	**product**	**Time (sec)**	**DP**	**EP**	**CE**	**CXP**
RS- and SR-EHBUP; RR-and SS-THBUP	242.0	168.0	115	0.0001	35	10	26	20

Supplemental Figure 1. MRM (A, B and D) and MS3 (C) trace chromatograms of diastereomers of bupropion metabolites BUP metabolites following direct injection of authentic standards to the LC/MS/MS system. 1, R-BUP; 2, S-BUP; 3, SS-OHBUP; 4, RR-OHBUP; 5, RS-EHBUP; 6, SR-EHBUP; 7, SS-THBUP; 8, RR-THBUP; and 9, nevirapine (internal standard). Abbreviation: OHBUP, hydroxyBUP; EHBUP, erythrohydroBUP; and THBUP, threohydroBUP.